

1  
2  
3  
4  
5  
6  
7  
8  
9  
10  
11  
12  
13  
14  
15  
16  
17  
18  
19  
20  
21  
22  
23  
24  
25  
26  
27  
28  
29  
30  
31  
32  
33  
34

---

**This pdf is a unformatted preprint of the final peer-reviewed version of the article in *Journal of Volcanology and Geothermal Research*. The DOI of the peer reviewed article is: 10.1016/j.jvolgeores.2022.107528**

**Article URL: <https://www.sciencedirect.com/science/article/pii/S0377027322000592>**

---

Persistent shallow micro-seismicity at Llaima volcano, Chile,  
with implications for long-term monitoring

Oliver D. Lamb<sup>a</sup>, Jonathan M. Lees<sup>a</sup>, Luis Franco-Marin<sup>b</sup>, Jonathan Lazo<sup>b,c</sup>, Andrés Rivera<sup>d</sup>, Michael J. Shore<sup>a</sup>, Stephen J. Lee<sup>e</sup>

<sup>a</sup>*Dept. of Earth, Marine and Environmental Sciences, University of North Carolina at Chapel Hill, Chapel Hill, NC, USA*  
<sup>b</sup>*OVDAS-Sernageomin, Chilean Geological Survey, Chile*  
<sup>c</sup>*Dept. of Physical Sciences, University of La Frontera, Temuco, Chile*  
<sup>d</sup>*Dept. de Geografía, Universidad de Chile, Chile*  
<sup>e</sup>*U.S. Army Research Laboratory/Army Research Office, Research Triangle Park, NC, USA*

---

**Abstract**

Identifying the source mechanisms of low-frequency earthquakes at ice-covered volcanoes can be challenging due to overlapping characteristics of glacially and magmatically derived seismicity. Here we present an analysis of two months of seismic data from Llaima volcano, Chile, recorded by the permanent monitoring network in 2019. We find over 2,000 repeating low-frequency events split across 82 families, the largest of which contains over 200 events. Estimated locations for the largest families indicate shallow sources directly beneath or near the edge of glaciers around the summit vent. These low-frequency earthquakes are part of an annual cycle in activity at the volcano that is strongly correlated with variations in atmospheric temperature, leading us to conclude that meltwater from ice and snow strongly affects the seismic source mechanisms related to glacier dynamics and shallow volcanic processes. The results presented here should inform future assessments of eruptive potential at Llaima volcano, as well as other ice-covered volcanoes in Chile and worldwide.

35 *Keywords:*

36 Volcano-seismology, Cryoseismology, Llaima volcano, Volcano monitoring

---

### 37 **Highlights**

- 38 • We investigate micro-seismic activity at Llaima volcano in early 2019.
- 39 • We observe dozens of families of persistent repeating earthquakes.
- 40 • Estimated locations suggest sources at shallow depths near or beneath glaciers.
- 41 • Long-term activity suggests strong relationship with snow and ice meltwater.

### 42 **1. Introduction**

43 Confident identification of recorded seismic signals and their source mechanisms  
44 is a fundamental aspect of assessing the eruptive potential of active volcanoes. Civil  
45 monitoring organizations and research groups must be prepared to recognize volcanic  
46 seismicity generated by fluid or magma ascent within volcanoes (Chouet and Matoza,  
47 2013). However, seismic monitoring of active ice-covered volcanoes is complicated by  
48 glacial processes (e.g. basal slip, crevassing, ice fall) generating signals greatly resembling  
49 those produced by volcanism, raising the risk of misidentification (Weaver and Malone,  
50 1976; Métaixian et al., 2003; Caplan-Auerbach and Huggel, 2007; Jónsdóttir et al., 2009;  
51 Thelen et al., 2013; Allstadt and Malone, 2014; Lamb et al., 2020). Therefore, detailed  
52 descriptions of glacial seismic sources at ice-covered active volcanoes is required before  
53 volcanic seismicity is used for assessing future eruption probability.

54 The Southern Chilean Volcanic Zone is home to >19 active ice-covered volcanoes that  
55 have erupted in recent history (Fig. 1, inset; Venzke, 2013). Llaima (3179 m a.s.l.) is  
56 one of the most active glacier-clad volcanoes in the region with up to 54 documented  
57 eruptions since the 17<sup>th</sup> century (Naranjo and Moreno, 2005; Franco et al., 2019). The  
58 most recent activity in 2007-09 generated 7 km tall ash plumes and lahars from melting  
59 of glacial ice (Franco et al., 2019). As of 2016, >14 km<sup>2</sup> of ice was present on almost all  
60 sides of the volcano edifice (Fig. 1; for a detailed description and discussion of how this  
61 glacial area was mapped, see Section 2 in Lamb et al., 2020). Most of these glaciers are  
62 thin (57 m maximum thickness in 2013; Gärtner-Roer et al., 2014) and retreating rapidly,  
63 with significant glacial area reductions in recent decades due to global climate change  
64 and eruptive activity (Reinthal et al., 2019).

---

*Email address:* olamb@email.unc.edu (Oliver D. Lamb)

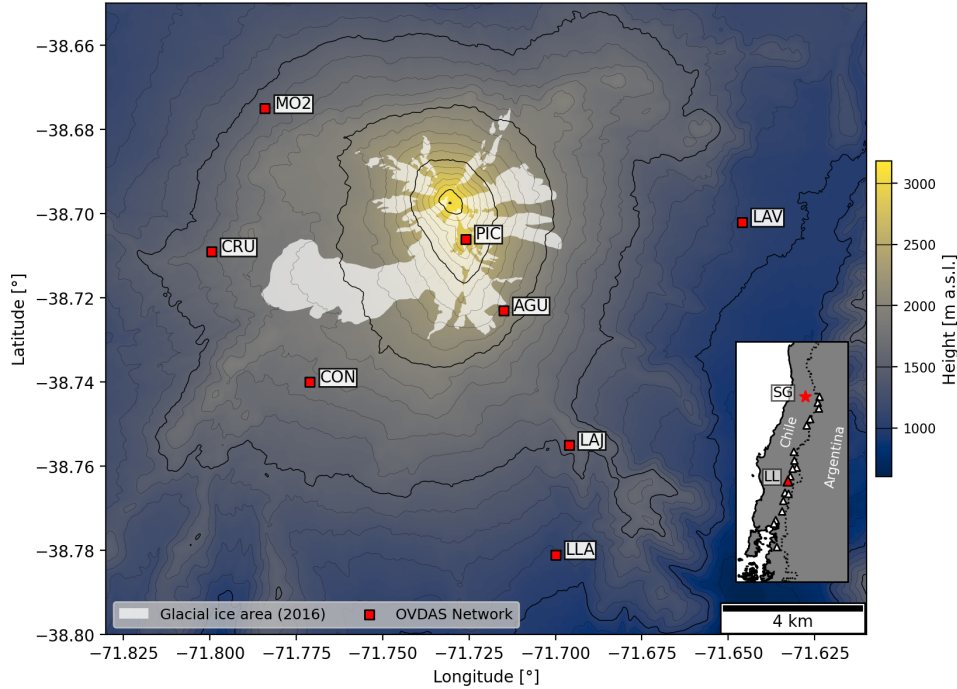


Figure 1: Map of Llaima volcano with the locations of OVDAS seismic stations (red squares) used in this study. Also marked are the mapped summit glacial areas which includes ‘debris-covered’ ice (white area). Thick and thin contours mark 500 and 100 m altitude intervals, respectively. Inset: Map of Southern Chile with the location of Llaima volcano (red triangle) and Santiago (red star, SG) marked. Also plotted are the locations of other ice-covered volcanoes within the Southern Volcanic Zone of Chile that have displayed eruptive activity in last 200 years (white triangles; Venzke, 2013).

65 Llaima is continuously monitored by OVDAS (Observatorio Volcanológico de los Andes  
 66 Sur<sup>1</sup>) who require timely and accurate identification of pre-eruptive seismic activity. The  
 67 challenge in identifying volcanic activity at the volcano was highlighted by Lamb et al.  
 68 (2020) that described multiple groups of low-frequency (<5 Hz) repeating earthquakes  
 69 during a two month period in early 2015. While a vast majority of these events were  
 70 apparently too low-amplitude to be documented in the OVDAS seismic record, their  
 71 low-frequency, repetitive nature resembles seismicity that can presage or accompany  
 72 eruptive activity (e.g. Chouet et al., 1994; Iverson et al., 2006; Kendrick et al., 2014; Lamb  
 73 et al., 2017). On the other hand, similar characteristics have been documented in seismic  
 74 activity attributed to glacial processes such as crevassing (e.g. Mikesell et al., 2012),  
 75 ice-fall (e.g. Jónsdóttir et al., 2009), hydrofracturing (e.g. Carmichael et al., 2012), and

<sup>1</sup>part of Servicio Nacional de Geología y Minería (SERNAGEOMIN)

76 basal slip (e.g. Thelen et al., 2013; Allstadt and Malone, 2014). After characterizing the  
77 families of repeating events at Llaima, Lamb et al. (2020) concluded they likely originated  
78 from basal slip at the ice-rock interface beneath the glaciers on the edifice. Key evidence  
79 to support this conclusion include mixed arrival polarities at various seismic stations, as  
80 well as shallow locations near or beneath glaciers around the volcano summit.

81 While the evidence described by Lamb et al. (2020) highlighted the potential for  
82 persistent glacial seismic activity at Llaima volcano, the study could not provide concrete  
83 conclusions to it's own questions. In particular, the results could not completely rule out  
84 other possible sources of repeating seismicity at the volcano, including slow-slip rupture  
85 of volcanic materials (e.g. Bean et al., 2013), resonance of fluid-filled cracks (e.g. Chouet,  
86 1996), and the interaction of snow and ice meltwater with magmatic hydrothermal fluids  
87 (e.g. Matoza et al., 2015; Park et al., 2019). Large error margins on locations for only a  
88 small number of repeating event families meant no strong conclusion could be made on  
89 the seismic source mechanism. Furthermore, the analysis of 2015 data raises the question  
90 of why was this persistent repeating seismic activity not previously documented? Llaima  
91 volcano has been instrumentally monitored by OVDAS since 1996 (Franco et al., 2019)  
92 and the glaciers on the edifice are supplemented by thick annual snowfall. Are the glaciers  
93 on the volcano changing (e.g. sliding faster) and the 2015 deployment was fortunate to be  
94 the first to record the repeating seismicity, or have these events been a long-term feature  
95 at the volcano but have been overlooked by previous studies?

96 In this study, we build on the findings of Lamb et al. (2020) by describing analysis of  
97 seismic data recorded in early 2019 over a similar two month period as in 2015. Here we  
98 aim to ascertain whether persistent, repetitive seismicity was recorded by the permanent  
99 OVDAS network during a two-month period in early 2019, using a similar but fine-tuned  
100 approach as the previous study. This includes using a different, amplitude-based location  
101 algorithm (instead of relative arrival times). We conclude by discussing the implications  
102 of our findings within the context of long-term seismic activity monitoring at Llaima, and  
103 how these events are likely related to variations in snow and ice meltwater.

## 104 **2. Data and Methodology**

### 105 *2.1. Data*

106 OVDAS are responsible for maintaining a network of seismometers around Llaima  
107 volcano, with 8 stations located within 10 km of the summit (Fig. 1). This includes  
108 two short-period, vertical component sensors (PIC and LAJ) and six broadband, three-  
109 component seismometers (AGU, CON, CRU, LAV, LLA and MO2), all recording and  
110 telemetered to OVDAS at 100 samples per second. The network around Llaima also  
111 includes stations designed to detect regional tectonic earthquakes and not volcanic

112 events (PA2, located 10.8 km SSE of LLA) or not available during the period of study  
113 due to technical issues (CNO, 2 km SSW of LAV), therefore neither of these stations  
114 were appropriate for use in this study. Additionally, weather data (temperature and  
115 precipitation) was monitored hourly at a station located in the town of Melipeuco (527  
116 m a.s.l., 17 km SSE of the volcano summit), maintained by the Agricultural Research  
117 Institute (INIA; data available via <https://agrometeorologia.cl/>, last accessed October  
118 2021). For this study, we use the data recorded from 1 February until 1 April 2019 by  
119 the eight stations described above and detailed in Fig. 1 and Table S1 in Supplementary  
120 Materials.

121 Earthquakes recorded by the network around the volcano are manually picked and  
122 catalogued by OVDAS, with waveform shapes, amplitudes, frequency characteristics  
123 and arrival times used to differentiate between volcanic and tectonic earthquakes. The  
124 majority of volcanic events are then divided into volcano-tectonic ( $>5$  Hz), long-period  
125 (0.5 - 5 Hz), or tremor events, and the temporal behaviour of each type has important  
126 implications for assessing the future eruptive potential of the volcano (see Chouet and  
127 Matoza, 2013, and references therein). Icequake events are also manually catalogued  
128 despite no mandate to do so, but until Lamb et al. (2020), few studies had analysed  
129 their recurrence in the seismic record (Mora-Stock et al., 2014); potential low amplitude  
130 icequakes would frequently be recognised at stations located close to the glaciers (e.g.  
131 AGU, Fig. S1 in Supp. Materials) but usually not catalogued. To assist with our study  
132 of the seismic record in early 2019, we use the OVDAS seismic event catalogue from 1  
133 February until 1 April 2019. The number of events catalogued by OVDAS during this  
134 period are described in the results section.

## 135 *2.2. Event detection*

136 To detect candidate seismic events at Llaima volcano in early 2019, we adopt a  
137 similar approach to that used in 2015 (Lamb et al., 2020). Trigger times were extracted  
138 from multiple stations using a short-term average/long-term average ratio (STA/LTA),  
139 on condition that an event was detected simultaneously at  $\geq 3$  stations in the OVDAS  
140 network. Window lengths of 0.7 and 8 s were used for the short- and long-term windows,  
141 respectively, with a ratio threshold of 3.5 used to define a detected event at each station.  
142 These parameters were decided using manual inspection of events detected over 24 hours  
143 of seismic data recorded at station AGU and differ from those used in 2015 (minimum 2  
144 stations, 1 and 9 s for short- and long-term windows, and a ratio threshold of 5). Seismic  
145 data during this step were pre-filtered with a 1-10 Hz bandpass filter to improve the  
146 signal-to-noise ratio (SNR). Lastly, the catalogue of triggers was combined with the  
147 catalogue of all seismic events manually compiled by OVDAS over the same time period,

148 with duplicates removed. This last step differs from the 2015 study (Lamb et al., 2020)  
149 which only used the OVDAS catalogue for comparison purposes.

### 150 *2.3. Identifying repeating events*

151 The next step is to find repetitive seismic events (i.e. families) within the catalogue  
152 of candidate seismic events compiled by the multi-station STA/LTA algorithm. This  
153 step follows a similar unsupervised clustering methodology to that used in Lamb et al.  
154 (2020) for the 2015 families, which is itself based on the approach used to recognise  
155 repeating events at Mt Rainier volcano (Carmichael, 2013; Allstadt and Malone, 2014).  
156 Each event is cross-correlated with all other events within each day, using a minimum  
157 cross-correlation coefficient of 0.8 to define 2 events as closely matching; this is higher  
158 than the 0.7 used for repeating events in 2015. The first 5 s of each event waveform is  
159 used, which is sufficient to maximise the SNR of each event. As station AGU had the  
160 highest number of detected events, waveforms from this station were used to build the  
161 catalogue of families. Families of repeating waveforms were defined using a hierarchical  
162 clustering method similar to that used by Buurman and West (2010) and Lamb et al.  
163 (2017); the `scipy.cluster.hierarchy` Python package is used for this step (For more  
164 details, see <https://docs.scipy.org/doc/scipy/reference/>, last accessed October 2021). In  
165 this approach, branches within the hierarchy are joined at nodes whose height is the mean  
166 cross-correlation value between each event pairs spanning the two groups. These nodes  
167 may join individual events or between clusters of events, depending on which linkage has  
168 the highest mean cross-correlation, and families are defined by nodes whose values are  
169 higher than a threshold.

170 Next, for each day a median waveform stack is computed for each family of 2 or  
171 more events, which are then compared with all other stacks across the whole time period  
172 to find larger, multi-day families. The last step ensures a more complete repeating  
173 event catalogue by using a frequency-domain approach with an overlap-add method,  
174 vectorization, and fast normalization to increase computation efficiency (SEC-C; Senobari  
175 et al., 2019). This step scans the entire time period with stacked waveforms from all  
176 multi-day and non-matched families (i.e. not multi-day) to find any events potentially  
177 overlooked in previous steps. This last step differs from Lamb et al. (2020) which only  
178 used multi-day families to scan for missed events, potentially underestimating the total  
179 number of families taking place in 2015.

### 180 *2.4. Event locations*

181 Arrival time location methods cannot be used on each individual event in each family  
182 as most are emergent and/or have onsets obscured by background noise. Since these  
183 events are repetitive, one option is to remove background noise by generating mean

184 waveforms (i.e. stacks) of the respective families at each station. This approach was  
185 effective in locating families of icequakes at Mt Rainier volcano (Allstadt and Malone,  
186 2014), but was less effective for similar events at Llaima in 2015 (Lamb et al., 2020).  
187 Large errors ( $\sim 500$  m) can be introduced by small offsets in stacking, which is difficult if  
188 the original events have low SNRs, or if the shallow velocity model for the area is not  
189 known. Here we adopt an approach which uses the full waveform instead of relying on  
190 relatively accurate arrival time measurements, and was originally developed for locating  
191 episodic tremor and slip in the northern Cascadian subduction zone (Wech and Creager,  
192 2008). Locations are estimated with a cross-correlation method that maximizes signal  
193 coherency among seismic stations within the network.

194 Centroid locations are estimated by cross-correlating all station pairs and performing  
195 a 3D grid search over potential source-location S-wave lag times that optimize the cross-  
196 correlations. The objective function  $M(x^{grid})$  is a weighted L1 norm on all pairs of  
197 cross-correlograms (Wech and Creager, 2008):

$$M(x^{grid}) = \sum_{i=1}^N \sum_{j=i+1}^N \frac{C_{ij}^{max} - C_{ij}(\delta t_{ij}(x^{grid}))}{\Delta C(C_{ij}^{max})} \quad (1)$$

198 where  $x^{grid}$  is a target source position,  $C^{ij}$  is the normalized cross-correlogram between  
199 the  $i$ th and  $j$ th functions,  $N$  is the number of seismograms,  $C_{ij}^{max}$  is the maximum value  
200 of the cross-correlogram, and  $\delta t_{ij}(x^{grid}) = t_i(x^{grid}) - t_j(x^{grid})$  is the predicted differential  
201 S-wave travel time between the  $i$ th and  $j$ th station using  $v_s = 2.5$  km.s<sup>-1</sup> (Franco et al.,  
202 2019); we assume the largest seismic amplitudes are generated during the arrival of  
203 S-waves at each station. Thus, for each possible grid location, we predict the lag time,  
204  $\delta t_{ij}(x^{grid})$ , between station pairs and evaluate its corresponding correlation value from  
205 the cross-correlogram  $C_{ij}(\delta t_{ij}(x^{grid}))$ . Traditional location methods seek solutions that  
206 minimize the time difference between predicted travel time and peak lag time, but this  
207 method instead minimizes the distance between the peak correlation,  $C_{ij}^{max}$ , and the  
208 predicted correlation,  $C_{ij}(\delta t_{ij}(x^{grid}))$ . Using only those observations with  $C_{ij}^{max} > 0.5$ , we  
209 maximize network coherency with respect to variations in  $x_{grid}$  by minimizing the sum  
210 over station pairs of this vertical correlation distance,  $C_{ij}^{max} - C_{ij}(\delta t_{ij}(x^{grid}))$  inversely  
211 weighted by the uncertainty  $\Delta C(C_{ij}^{max})$ .

212 The above calculation was performed within the ‘envelop’ Python package (Wech  
213 and Creager, 2008). This optimization problem was performed on a grid with  $0.005^\circ$   
214 lateral and 100 m depth intervals (down to 5 km) centered on the summit of the volcano.  
215 However, the ‘envelop’ package was originally developed for searching for locations across  
216 a much larger area than that which is used here so topography was previously not taken  
217 into account, and stations were located at the top of the grid (i.e. the surface). With a

218 vertical difference of  $\sim 1800$  m between stations 7 km apart (PIC and LLA), we customized  
219 the grid location search to account for the sharp topography around Llaima volcano. The  
220 top of the grid is set as the summit of the volcano, and each station was then embedded  
221 within the grid at the relevant coordinates and depth. Each grid point was then compared  
222 to a topographic map, all points above the topography were excluded and the remaining  
223 grid point with the lowest misfit, defined as  $C_{ij}^{max} - C_{ij}(x^{best})$ , was picked as the source  
224 location. Centroid location results at or too close to the edge of the search grid were  
225 rejected.

### 226 2.5. Qualitative event magnitude estimation

227 For each family successfully located on Llaima volcano we can also estimate their  
228 individual event magnitudes, assuming that each family is derived from a fixed location.  
229 Event magnitudes, together with characteristic frequencies, of glacially derived seismicity  
230 may also provide evidence towards the source mechanism of each family (Podolskiy and  
231 Walter, 2016). Magnitudes for long-period and tremor events detected at Llaima by  
232 OVDAS are not routinely calculated (the reduced displacement is calculated instead),  
233 therefore we adopt an approach previously used for qualitatively estimating magnitudes of  
234 micro-seismic events detected at Hekla volcano, Iceland (Eibl et al., 2014). This approach  
235 uses recorded amplitudes of located regional seismic events to estimate the magnitudes of  
236 local events using their source amplitudes. The 37 regional events used here were recorded  
237 and documented by Centro Sismológico Nacional (CSN) and OVDAS, occurring up to  
238 250 km from Llaima volcano, up to depths of 113 km, at azimuths between 170 and 30°,  
239 and with calculated local magnitudes of 0.5 – 4.0 (Table S2 and S3 in Supp. Material).

240 Before estimating magnitudes, site effects must be removed from the recorded seismic  
241 data at each station. Coda waves can be used to estimate site amplification (Aki and  
242 Ferrazzini, 2000; Battaglia and Aki, 2003; Kumagai et al., 2010; Eibl et al., 2014). For  
243 each regional event recorded by CSN and OVDAS we used a 30 s time window that begins  
244 at  $2t_s$ , where  $t_s$  is the estimated arrival time of S-waves at each station. Each waveform  
245 was instrument corrected and bandpass filtered to 1 – 10 Hz before root mean square  
246 values in 5 s, non-overlapping windows were calculated (Aki, 1969). All RMS values were  
247 averaged and compared to the chosen reference station, MO2. This station was selected  
248 as the reference station as it had the least interrupted seismic dataset and least local high  
249 frequency background noise. The resulting correction factors are provided in Table S1 in  
250 Supplementary Materials.

251 To estimate source amplitudes for each of the regional events, we first remove the site  
252 amplification and instrument response, before filtering to 1 – 10 Hz. The maximum of  
253 the smoothed Hilbert Transform was used as maximum amplitude  $A_i$  at each station  $i$ .



254 The amplitude at the source,  $A_0$ , was then calculated at each station based on (Battaglia  
255 and Aki, 2003)

$$A_{0_i} = \frac{A_i r_i}{e^{-B r_i}} \quad (2)$$

256 with

$$B = \frac{\pi f}{Q \beta} \quad (3)$$

257 where  $r$  is the source-to-receiver distance,  $f$  is the central frequency,  $\beta$  is wave velocity  
258 ( $2.5 \text{ km.s}^{-1}$ ), and  $Q$  is the quality factor for attenuation (100; Eibl et al., 2014). A linear  
259 regression was then implemented with the logarithm of the mean source amplitudes  
260 versus the published local magnitudes. Finally, to estimate the local magnitudes of the  
261 events detected in this study at Llaima, we first calculate their source amplitudes using  
262 estimated source location of each family of repeating events, under the assumption that  
263 families of repeating events are derived from a relatively fixed source location. These  
264 source amplitudes were then converted to a local magnitude using the regression line  
265 calculated using regional events.

### 266 3. Results

#### 267 3.1. Seismic activity

268 Between 1 February and 1 April 2019, we detected 6,647 seismic events at Llaima  
269 volcano (Fig. 2a). Higher numbers of events were detected at stations closer to the  
270 summit, and hourly rates of detections appear to show a diurnal variation that is inversely  
271 correlated with background seismic noise levels (Fig. S3). During the same time period,  
272 OVDAS manually catalogued a total of 967 events, including 666 long-period, 1 volcano-  
273 tectonic, 271 rockfall, and 29 icequakes (Fig. 2c, S2). Using the catalogue of automatic  
274 detections, we identified 2,006 repeating events across 82 families (Fig. 2b, 3). Of these,  
275 370 events were already featured in the OVDAS catalogue, including 270 classified as  
276 long-period events. The largest of these families contained 207 events (Family 5; Fig. 3).  
277 The daily rate of seismicity, including repeating events, show no obvious indications of  
278 cyclic activity or significant changes in rates except for 18 March. On that date, a peak in  
279 seismic activity (not seen in repeating events; Fig. 2b) occurs shortly after a brief period  
280 of rainfall recorded at the town of Melipeuco, approximately 17 km SSE of the volcano  
281 summit (Fig. 2d).

#### 282 3.2. Locations

283 Locations were estimated for all families containing at least 30 seismic events ( $n=17$   
284 , highlighted with blue diamonds in Fig. 3). Due to low SNRs for individual events,

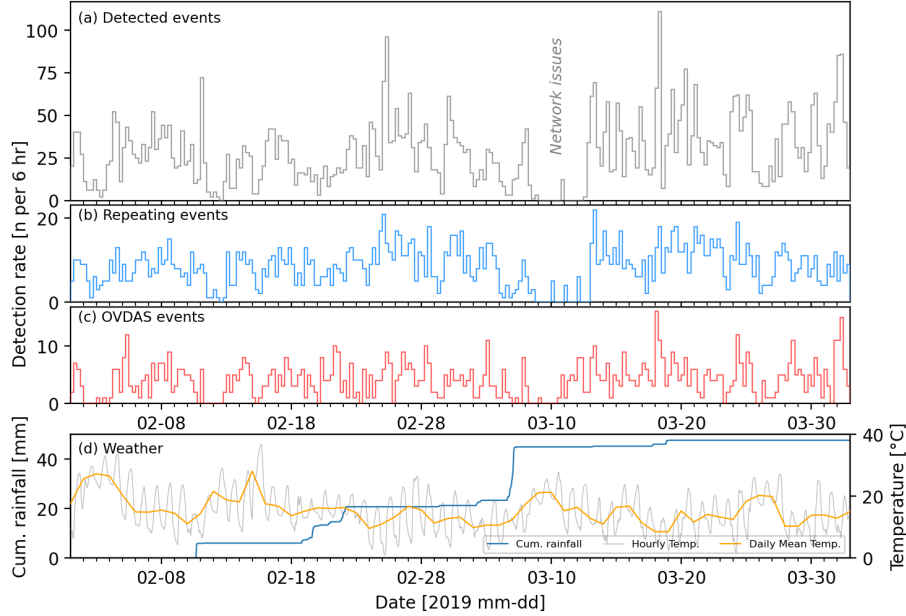


Figure 2: Rates for (a) events automatically detected, (b) events classified as repeaters, and (c) seismic events manually classified by OVDAS from 1 February to 1 April 2019 in 3-hour bins. (d) Cumulative rainfall (blue line) and variations in temperature on an hourly (grey) and daily rate (orange line) at the weather station located in Melipeuco.

285 locations could only be reliably estimated using mean waveforms for each family at each  
 286 station, generated by stacking waveforms of all events. An example of an estimated  
 287 location is given in Figure 4 for family 4; see Figs. S5 - S20 in the supplementary materials  
 288 for all other locations. Out of the 17 families for which locations were estimated, 5 were  
 289 rejected due to locations at or too close to the edge of the search grid (Families 10, 19, 36,  
 290 71, and 73; Figs. S11, S13, S17, S20 and S21, respectively). The remaining 12 families  
 291 are all located at shallow depths ( $<500$  m) around the summit of the volcano (Fig. 5).  
 292 Note that 5 of these families are located at or within close approximation to each other  
 293 (Families 2 and 64, and Families 16, 21, and 32). With the exception of family 7, all  
 294 located families were located directly beneath or at the edge of mapped glacial areas  
 295 around the summit of the volcano.

### 296 3.3. Qualitative magnitude estimates

297 Local magnitudes were estimated for each event within all families for which locations  
 298 could be calculated (Fig. 5). Local magnitudes for all located repeating events fell  
 299 within the 0.9 – 1.5 range, with little distinct difference between families (Fig. 6). As we

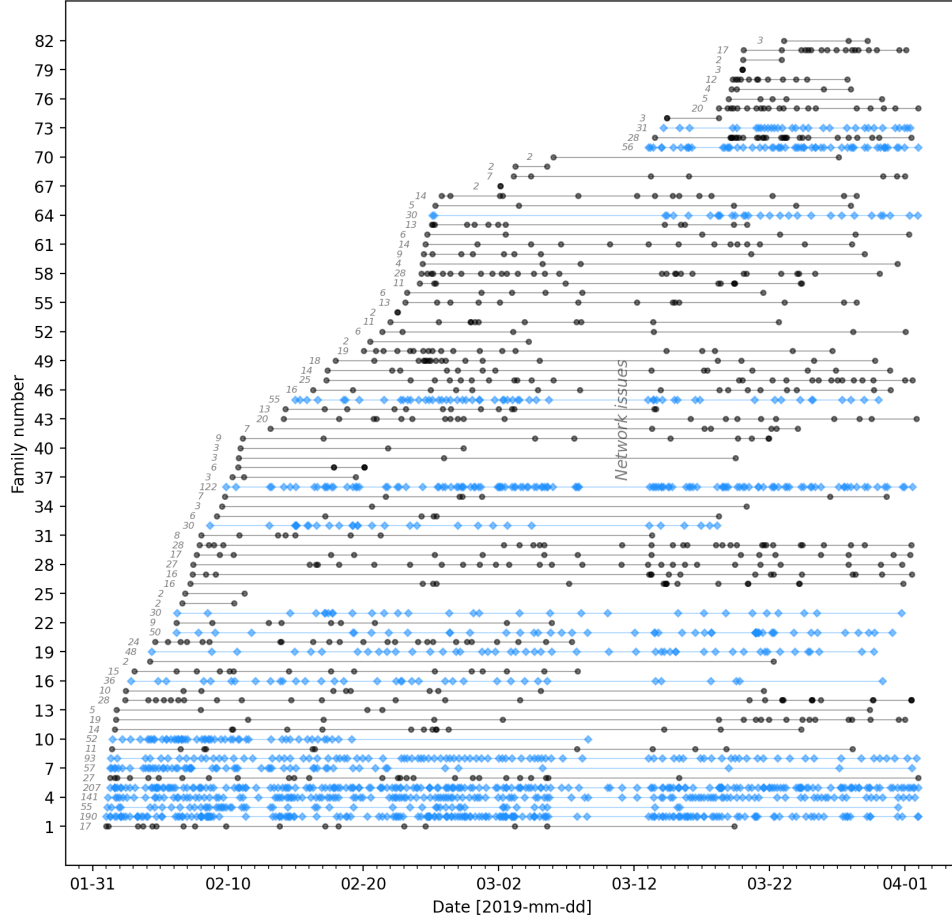


Figure 3: Catalogue of family occurrence in our dataset. Each plotted point represents the time of an event, and lines join events from the same family. The total number of events in each family is noted with grey numbers before the first event. Families containing 30 or more events are highlighted using blue diamonds for the individual events.

300 assumed straight wave propagation between source and receiver, we underestimate  $A_0$  for  
 301 regional events which, in turn, implies that local magnitudes for all repeating events are  
 302 overestimated; therefore, the values calculated here represent a maximum feasible value.

#### 303 4. Discussion

304 Here we have presented results from detailed analysis of seismic data collected at  
 305 Llama volcano in early 2019, with the aim of building on previous work (Lamb et al.,  
 306 2020) to understand the prevalence of icequakes from glaciers around the summit. The

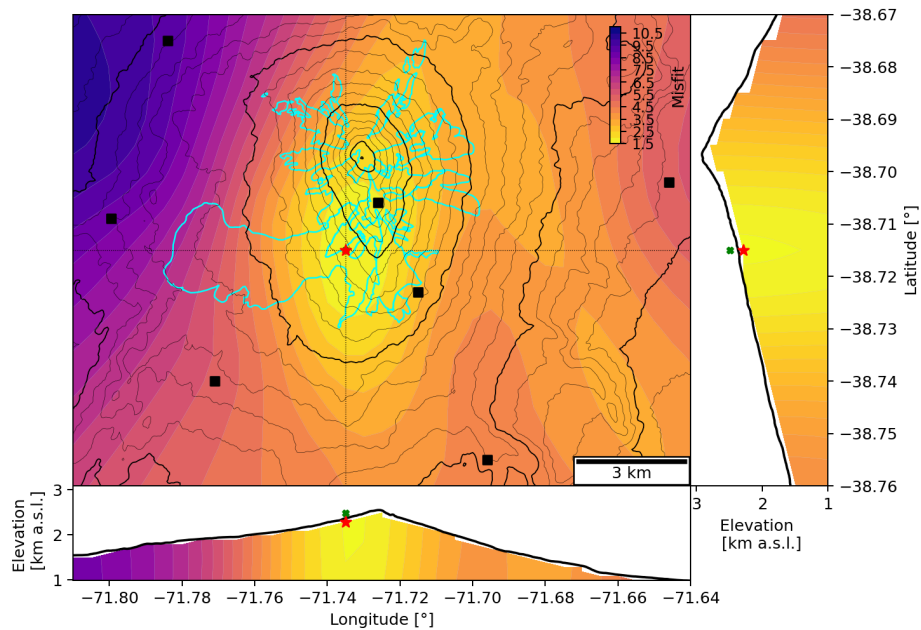


Figure 4: Example output of location method used, here illustrating the location of Family 4 (red star). The green square in each cross section panel (right and bottom) shows the location if topography was not accounted for. Dotted lines indicate the profiles of the cross-section panels (right and bottom), centred on the final location of the family. Blue lines on main panel outline the mapped summit glacial areas. Black squares are locations of OVDAS seismic stations.

307 key differences from Lamb et al. (2020) is this study uses seismic data from the permanent  
 308 OVDAS monitoring network around the volcano (Fig. 1), a new approach for calculating  
 309 event locations that does not rely on accurate arrival time picks, as well as a first attempt  
 310 at quantifying local magnitudes of the repeating seismic events.

311 The persistent repeating seismicity observed in 2015 (Lamb et al., 2020) appears  
 312 to be continuing in 2019, albeit with higher numbers of detected events (Fig. 2a, b).  
 313 Consequently, these observations answer the questions posed in the introduction by  
 314 suggesting that persistent repeating seismic activity is a long-term feature at Llaima  
 315 volcano. The elevated levels of activity in 2019 relative to 2015 is reflected by the higher  
 316 number of manually catalogued events by OVDAS (Fig. 2c), with 967 events in 2019  
 317 compared to 490 in 2015. Furthermore, the seismic activity in 2019 appears to show  
 318 no relation to changes in weather (Fig. 2d) which was also observed in 2015 (Lamb  
 319 et al., 2020). One key difference between 2019 and 2015 is that the number of families of  
 320 repeating events is much greater in the former than the latter time period, with 82 and  
 321 11, respectively. This is likely due to a slightly different criteria for classifying families in  
 322 each analysis, in particular, with the 2015 study only using stacks from multi-day families

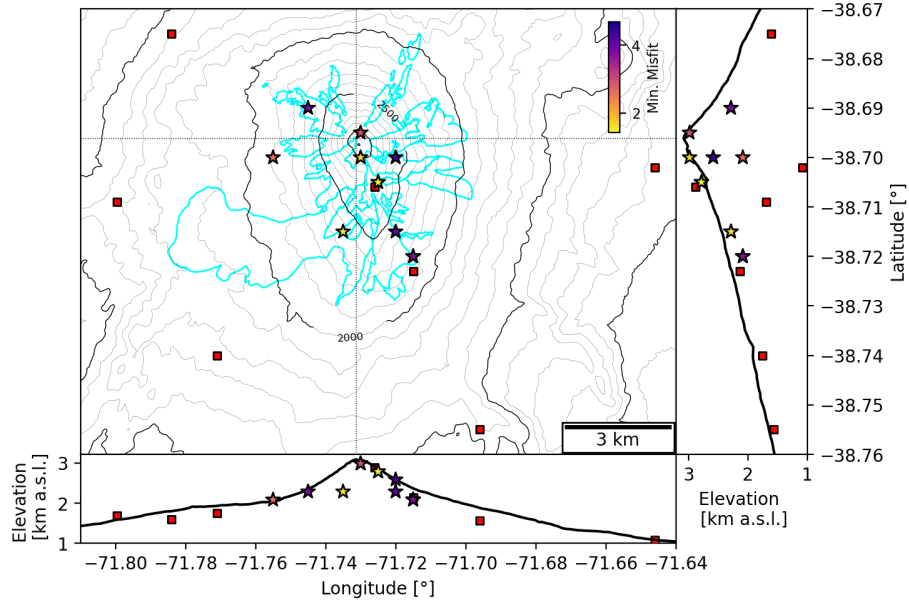


Figure 5: Results for all families that were located (stars). Each star is coloured by the minimum misfit for their location. Dotted lines indicate the profiles of the cross-section panels (right and bottom), centred on the summit of the volcano. Red squares indicate the location of OVDAS seismic stations, and blue lines outline the mapped summit glacial areas.

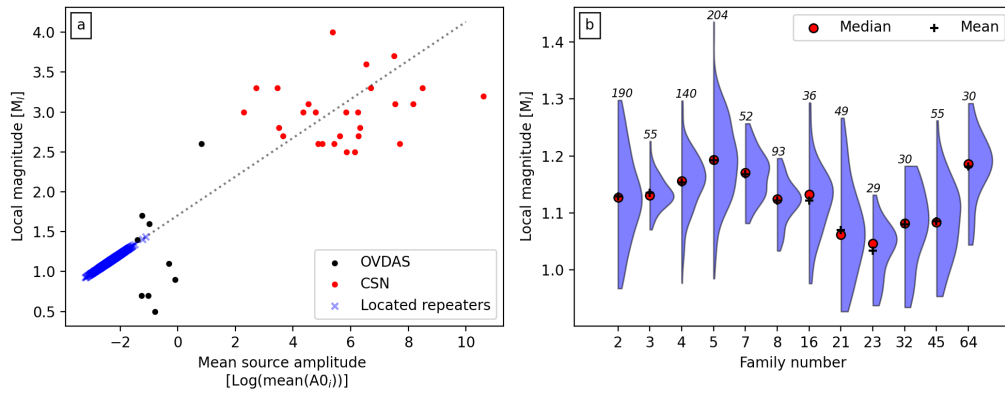


Figure 6: Results of qualitative local magnitude estimates. (a) Local magnitudes of located repeating events in this study (blue cross) estimated using the linear regression (dotted line) calculated from regional events detected by CSN (red dots) and OVDAS (black dots). (b) Half-violin plots for each located family showing their distribution of estimated local magnitudes with rotated kernel density plots (blue). Also plotted is the median (red circle) and mean (black cross) of the local magnitude for each family. Numbers above each half-violin plot indicate the total number of events within each family.

323 to scan for missed events with the SEC-C algorithm (Senobari et al., 2019). If we use the  
324 same criteria in 2019 as that used in 2015, we find only 12 families in total (not shown  
325 here).

326 Compared to 2015, the new approach for calculating locations of repeating events  
327 is more successful in 2019 (Fig. 5). The results suggest that the locations of all the  
328 largest detected families are shallow ( $<100$  m) and almost all beneath or near the edge of  
329 glaciers around the summit of Llaima volcano, with the sole exception being family 7 (Fig.  
330 S9). These location estimates represent an improvement on those in 2015, with a greater  
331 number of families located and more robust estimation of location errors. However, there  
332 remain significant errors (represented here by the misfit) in locations, particularly in the  
333 vertical component (e.g. see cross-section panels in Fig. 4). This is due to the use of  
334 a 1D velocity model for Llaima volcano, as no shallow 2D velocity model is currently  
335 available for the volcano. We assessed the sensitivity of the location estimations to the  
336 chosen seismic velocity ( $2.5 \text{ km.s}^{-1}$ ) by re-estimating locations with three other possible  
337 velocities ( $1.25$ ,  $2.0$  and  $3.0 \text{ km.s}^{-1}$ ). Results indicate that while locations may change,  
338 they remain within the lowest uncertainty levels indicated by the location misfits of the  
339 original locations (Fig. S22 - S24). Furthermore, the depths of the locations generally  
340 remain in the shallow depths of the upper edifice. Therefore, the estimated locations  
341 and depths for most families support the hypothesis that these were generated by glacial  
342 activity rather than volcanic.

343 Qualitative event magnitudes for each located family suggest little distinct differences  
344 in energies between families (Fig. 6). The lack of obvious differences between each family  
345 suggests they may be generated by a similar source mechanism, but at different locations.  
346 A review of glacial seismicity has suggested that source mechanisms may be identified  
347 via their frequency versus magnitude relationship (see Fig. 14 in Podolskiy and Walter,  
348 2016). For the repeating events for which we have estimated their local magnitudes,  
349 their central frequencies lie in the range of  $3.5$  to  $6.5$  Hz which would be associated with  
350 stick-slip activity at the base of glaciers. Similar frequencies were observed for basal  
351 stick-slip events at Iliamna and Mt Rainier volcanoes (Caplan-Auerbach et al., 2004;  
352 Caplan-Auerbach and Huggel, 2007; Allstadt and Malone, 2014), but the magnitudes  
353 estimated at Llaima ( $M_l 1 - 1.2$ ; Fig. 6) are higher but likely represent overestimates  
354 due to an underestimation of  $A_0$  for regional seismic events. The relatively thin ice  
355 thicknesses on Llaima volcano (maximum  $57$  m in 2013; Gärtner-Roer et al., 2014) may  
356 preclude the occurrence of stick-slip activity due to insufficient normal stresses. However,  
357 we argue that the steepness of volcano edifice provides conditions to induce stick-slip  
358 activity at the base of the glaciers, as indicated by the locations of families on the steepest  
359 parts of the edifice (see cross-section panels in Fig. 5). Alternative glacial processes for

360 generating repetitive icequakes include englacial crevassing (e.g. Mikesell et al., 2012),  
361 hydrofracturing (e.g. Carmichael et al., 2012), and ice-fall (e.g. Jónsdóttir et al., 2009).  
362 Crevassing is considered an unlikely process as it releases very little seismic energy and is  
363 typically only detected by seismic stations directly on the ice or on rock very close by  
364 (Weaver and Malone, 1979; Thelen et al., 2013; Allstadt and Malone, 2014). Furthermore,  
365 steep glaciers are poorly coupled to their bed and therefore do not efficiently transmit  
366 seismic waves outside the ice (Kamb, 1970; Weaver and Malone, 1979). Hydrofracturing  
367 is not considered a major process for the families in 2019 as there was no clear evidence  
368 for harmonics or consistent spectral peaks across the seismic stations (not shown here),  
369 though the resonant nature of signal could be lost due to waveform alteration between  
370 source and receiver. Finally, we also exclude ice-fall because, as noted in Lamb et al.  
371 (2020), there are no documented areas that host persistent, highly-repetitive glacial ice  
372 collapse around Llaima volcano.

373 The estimation of locations (and in turn, the event magnitudes) using waveform stacks  
374 assumes that the source for each event within each family remains fixed. Geller and  
375 Mueller (1980) suggest highly correlated waveforms such as those found in repeating event  
376 families must be within a quarter wavelength so as to not be influenced by the structure  
377 between two source locations. Central frequencies for events within the largest families  
378 range from 3.5 to 6.5 Hz which, together with  $v_s = 2.5 \text{ km.s}^{-1}$ , suggest the spread of  
379 locations should be no more than approximately 96 to 179 m. However, cross-correlations  
380 between all events relative to the first detected event highlight a gradual de-correlation  
381 over the lifespan of each family (Fig. S4; note these are not the same cross-correlation  
382 values used to assign events into families). A similar observation was made for icequake  
383 families at Mt Rainier volcano (Thelen et al., 2013) and is likely the result of either  
384 changes in source mechanism, modifications to the source-receiver pathway, or the slow  
385 migration of the source over time. Here we favour the latter option, considering the  
386 other options would likely give abrupt changes in correlation over time, not somewhat  
387 continuous. For example, significant precipitation events at Mt Rainier produced abrupt  
388 but short-lived reductions in cross-correlation values (See Fig. 5 in Thelen et al., 2013).

389 Before conclusions can be drawn from short-term observations and analysis, the  
390 results from this study as well as Lamb et al. (2020) must be placed in the context of  
391 the long-term seismic activity of Llaima volcano (Fig. 7). From 1 January 2013 to 31  
392 December 2020, a total of 11,079 LP earthquakes were cataloged at Llaima volcano and  
393 daily event rates over that time show a clear annual fluctuation with higher event rates in  
394 the austral summer (December to April) versus the winter (May to November; Fig. 7a).  
395 Over the same time period, volcanic activity at Llaima was minimal aside from a brief but  
396 intense swarm of volcanic LP events from 1-3 October 2017, peaking with 460 events on 2

397 October (Fig. 7a). A visual comparison with daily weather measurements from a station  
398 located in Melipeuco (Fig. 7b) shows an apparent positive correlation with temperature  
399 and negative correlation with rainfall. To quantify this relationship, we performed a  
400 normalised cross-correlation between temperature, rainfall and wind velocities and the  
401 rate of LP earthquakes. To assess the significance of the correlation values, we followed  
402 Allstadt and Malone (2014) by performing 5000 cross correlations between randomised  
403 weather data and the earthquake data to estimate the maximum cross-correlation value  
404 that could be found by random chance. The resulting correlations with temperature  
405 and rainfall oscillate with a period of approximately one year, with rainfall oscillating  
406 negatively (Fig. 7c); correlations with wind velocity show no clear annual oscillation.  
407 Only temperature has a peak (0.32) which exceeds the maximum correlation value that  
408 could be obtained randomly (0.3). There is also a strong diurnal cycle in event rates  
409 from 2013 to 2020 with lower detection rates from 1000 to 1800 local time (Fig. 7d).  
410 Visual comparison with hourly wind and temperature data suggests this is possibly due  
411 to increased seismic noise from wind drowning out smaller magnitude events (Fig. 7d). A  
412 similar observation was made during the analysis of seismic events related to the glaciers  
413 on Cotopaxi volcano (Métaxian et al., 2003). Alternatively, higher rates of seismic activity  
414 during night-time hours may be due to nocturnal thermal fracturing of ice (Carmichael  
415 et al., 2012; Podolskiy et al., 2018, 2019) or nightly reductions in surface melt input  
416 causing increased basal pressure and traction (Carmichael et al., 2015). Measurements of  
417 background seismic noise during the 2019 period of study suggest elevated levels of wind  
418 during daytime hours (Fig. S3), therefore we do not favour these alternative processes to  
419 explain the diurnal variations; however, we cannot completely rule out these processes  
420 taking place at Llaima volcano.

421 Annual cycles in seismic activity correlating with variations in precipitation or tem-  
422 perature have been observed at other ice- and snow-covered volcanoes (Jónsdóttir et al.,  
423 2009; Allstadt and Malone, 2014; Park et al., 2019; Castaño et al., 2020). Low-frequency  
424 earthquakes at volcanoes can be triggered by rainfall (e.g. Matthews et al., 2009) or  
425 snowfall (Allstadt and Malone, 2014) however LP activity at Llaima is inversely correlated  
426 with precipitation and positively correlated with temperatures (Fig. 7c). Therefore, we  
427 interpret the annual cycle in activity at Llaima as the result of yearly melting of snow and  
428 ice around the summit of the volcano. An increase in meltwater at the surface can increase  
429 the recurrence of basal slip beneath glaciers at the ice-rock interface. Fluctuations in  
430 meltwater flow can directly modulate the recurrence of basal slip beneath glaciers due  
431 to changes in shear strength with effective pressure (e.g. Mikesell et al., 2012; Roeoesli  
432 et al., 2016; Nanni et al., 2020). Percolation of meltwater into the shallow subsurface of  
433 Llaima volcano may also increase the recurrence of slow-slip failure of critically stressed



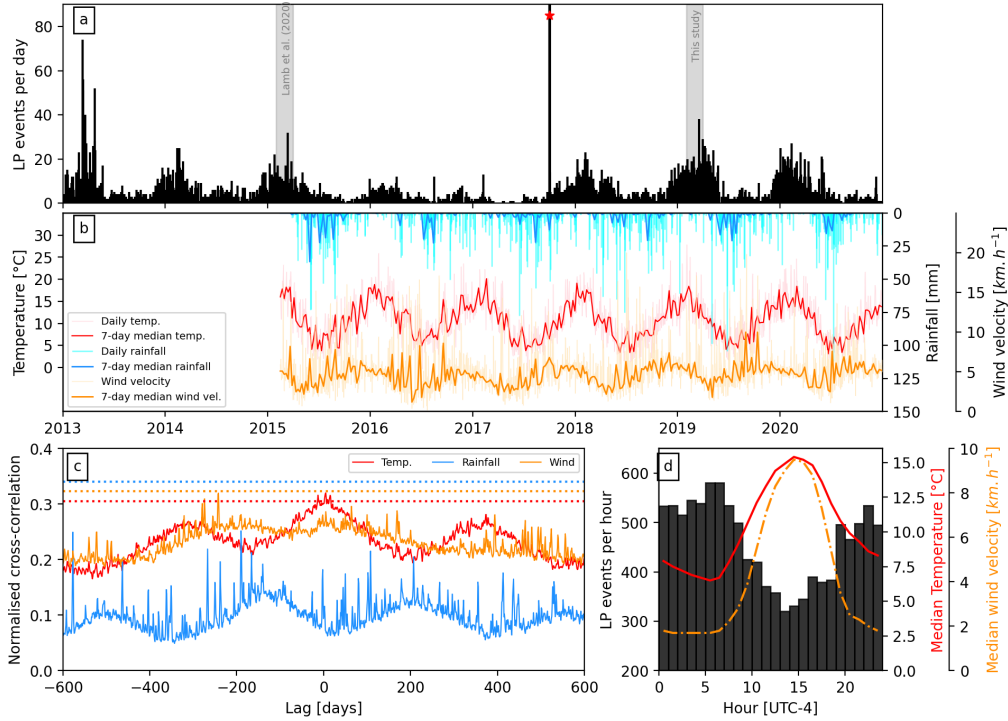


Figure 7: Long-term seismic activity and weather at Llaima volcano. (a) Number of LP seismic events manually catalogued per day by OVDAS at Llaima volcano from 1 January 2013 to 31 December 2020. Grey areas mark time periods studied in Lamb et al. (2020) and this study. Red star marks time period of intense volcanic LP activity observed at Llaima volcano. (b) Daily and 5-day median temperature (grey and red lines) and precipitation (cyan bars and green line) measurements from weather station located in Melipeuco, 8 km south of station LLA. Weather data is not available prior to 15 February 2015. (c) Normalised cross correlation between daily LP seismic events (after 15 February 2015) and temperature (red), rainfall (blue) and wind velocity (orange). Horizontal dotted lines indicate the maximum correlation obtained when temperature (red), rainfall (blue) and wind velocity (orange) data were randomized and correlated against the earthquake data 5000 times. (d) Histogram of LP event rates by hour from 2013 to 2020 (black bars), plotted with median temperature (red) and wind velocity (dashed orange) per hour of day.

434 fractures within poorly consolidated volcanic material (e.g. Bean et al., 2013; Heap  
 435 et al., 2015). However, experimental observations suggest such a mechanism is unlikely  
 436 (but not impossible) to generate repetitive seismicity like those observed in 2015 and  
 437 2019 at Llaima (Heap et al., 2015). The ingress of meltwater into the edifice may also  
 438 lead to the excitation of repetitive low magnitude LP events caused by sudden pressure  
 439 changes within a shallow hydrothermal system. A similar mechanism was suggested for  
 440 low-frequency seismic activity at Nevado del Ruiz and Mount St Helens volcanoes (Leet,  
 441 1988; Matoza et al., 2015) as well as for causing annual seismic cycles at Ngauruhoe

442 volcano (New Zealand; Park et al., 2019). Petrological analysis of eruptive products from  
443 Llaima volcano has suggested that magma is stored at very shallow depths ( $\leq 4$  km) as a  
444 series of dyke intrusions beneath the summit vent where they undergo intense degassing  
445 between eruptions (de Maisonneuve et al., 2012; Ruth et al., 2016, 2018). Therefore, it  
446 is possible that a shallow hydrothermal system is present within Llaima volcano and is  
447 interacting on an annual basis with snow and ice meltwater.

448 Identifying specific source mechanisms for each of the repeating families described in  
449 this study is difficult due to the low signal-to-noise ratios of the seismic signals. However,  
450 evidence from locations, local magnitudes, and drifting source locations suggest that the  
451 majority of background long-period seismic activity is generated by basal slip beneath the  
452 glaciers. Nevertheless, due to the large number of identified families (Fig. 3) it may be  
453 reasonable to conclude that all three of the mechanisms affected by meltwater (increased  
454 basal slip, slow-slip failure of volcanic material, and interaction with hydrothermal system)  
455 may be occurring at Llaima volcano.

## 456 5. Conclusions

457 Rigorous interpretation of the source mechanisms of low-frequency earthquakes is  
458 vital for assessing the future eruptive potential of ice-covered volcanoes, particularly  
459 as icequakes can share many characteristics with volcanic long-period events. Here we  
460 present a detailed analysis of two months of seismic data recorded at Llaima volcano,  
461 Chile, in 2019. Over 2,000 repeating low-frequency earthquakes were identified across 82  
462 different families, the largest of which contained over 200 events and was persistent for the  
463 whole time period of analysis. Locations of the largest families indicate shallow sources  
464 near or directly beneath glaciers present around the summit of the volcano. Long-term  
465 seismic activity reveals that these repeating seismic events are part of an annual seismic  
466 cycle that is strongly correlated with atmospheric temperature. Therefore, we conclude  
467 that the low-frequency repeating events seen at Llaima volcano are triggered by variations  
468 in meltwater affecting basal slip beneath the glaciers, as well as interactions with critically  
469 stressed fractures and a shallow hydrothermal system within the edifice. The details of  
470 the study presented here should inform future decision making during seismic crises at  
471 Llaima volcano as well as other ice-covered volcanoes in Chile and globally.

## 472 Acknowledgments

473 This research was performed while ODL held an NRC Research Associateship with  
474 the U.S. Army Research Laboratory/Army Research Office while based at the University  
475 of North Carolina at Chapel Hill. The authors wish to thank all analysts at OVDAS

476 who were involved in performing routine manual cataloging of seismic activity at Llaima  
477 volcano and whose work was valuable for this analysis. In addition, we would like to  
478 thank Evgeny Podolskiy and an anonymous reviewer for their comments and suggestions  
479 which greatly improved the manuscript.

#### 480 **Declaration of Interests Statement**

481 The authors declare that they have no known competing financial interests or personal  
482 relationships that could have appeared to influence the work reported in this paper.

#### 483 **Bibliography**

- 484 Aki, K., 1969. Analysis of the seismic coda of local earthquakes as scattered waves. *Journal of Geophysical*  
485 *Research* 74, 615–631. doi:10.1029/JB074i002p00615.
- 486 Aki, K., Ferrazzini, V., 2000. Seismic monitoring and modeling of an active volcano for prediction.  
487 *Journal of Geophysical Research: Solid Earth* 105, 16617–16640. doi:10.1029/2000JB900033.
- 488 Allstadt, K.E., Malone, S.D., 2014. Swarms of repeating stick-slip icequakes triggered by snow loading at  
489 Mount Rainier volcano. *Journal of Geophysical Research: Earth Surface* 119, 1180–1203. doi:10.1002/  
490 2014JF003086.
- 491 Battaglia, J., Aki, K., 2003. Location of seismic events and eruptive fissures on the Piton de la  
492 Fournaise volcano using seismic amplitudes. *Journal of Geophysical Research* 108, 2364. doi:10.1029/  
493 2002JB002193.
- 494 Bean, C.J., De Barros, L., Lokmer, I., Métaixian, J.P., O’ Brien, G., Murphy, S., 2013. Long-period  
495 seismicity in the shallow volcanic edifice formed from slow-rupture earthquakes. *Nature Geoscience* 7,  
496 71–75. doi:10.1038/ngeo2027.
- 497 Burman, H., West, M.E., 2010. Seismic Precursors to Volcanic Explosions During the 2006 Eruption of  
498 Augustine Volcano. p. 41–57.
- 499 Caplan-Auerbach, J., Huggel, C., 2007. Precursory seismicity associated with frequent, large ice avalanches  
500 on Iliamna volcano, Alaska, USA. *Journal of Glaciology* 53, 128–140. doi:10.3189/172756507781833866.
- 501 Caplan-Auerbach, J., Prejean, S.G., Power, J.A., 2004. Seismic recordings of ice and debris avalanches of  
502 Iliamna Volcano, Alaska. *Acta Vulcanologica* 16, 9–20.
- 503 Carmichael, J.D., 2013. Melt-triggered seismic response in hydraulically-active polar ice: Observations  
504 and methods. Ph.D. thesis. University of Washington.
- 505 Carmichael, J.D., Joughin, I., Behn, M.D., Das, S., King, M.A., Stevens, L., Lizarralde, D., 2015.  
506 Seismicity on the western greenland ice sheet: Surface fracture in the vicinity of active moulins:  
507 Seismicity near moulins, w greenland. *Journal of Geophysical Research: Earth Surface* 120, 1082–1106.  
508 doi:10.1002/2014JF003398.
- 509 Carmichael, J.D., Pettit, E.C., Hoffman, M., Fountain, A., Hallet, B., 2012. Seismic multiplet response  
510 triggered by melt at blood falls, taylor glacier, antarctica. *Journal of Geophysical Research: Earth*  
511 *Surface* 117. doi:10.1029/2011JF002221.
- 512 Castaño, L.M., Ospina, C.A., Cadena, O.E., Galvis-Arenas, B., Londono, J.M., Laverde, C.A., Kaneko,  
513 T., Ichihara, M., 2020. Continuous monitoring of the 2015–2018 Nevado del Ruiz activity, Colombia,  
514 using satellite infrared images and local infrasound records. *Earth, Planets and Space* 72, 81. doi:10.  
515 1186/s40623-020-01197-z.

- 516 Chouet, B.A., 1996. Long-period volcano seismicity: its source and use in eruption forecasting. *Nature*  
517 380, 309–316. doi:10.1038/380309a0.
- 518 Chouet, B.A., Matoza, R.S., 2013. A multi-decadal view of seismic methods for detecting precursors  
519 of magma movement and eruption. *Journal of Volcanology and Geothermal Research* 252, 108–175.  
520 doi:10.1016/j.jvolgeores.2012.11.013.
- 521 Chouet, B.A., Page, R.A., Stephens, C.D., Lahr, J.C., Power, J.A., 1994. Precursory swarms of long-  
522 period events at Redoubt Volcano (1989-1990), Alaska: Their origin and use as a forecasting tool.  
523 *Journal of Volcanology and Geothermal Research* 62, 95–135.
- 524 Eibl, E.P., Bean, C.J., Vogfjörð, K., Braiden, A., 2014. Persistent shallow background microseismicity on  
525 Hekla volcano, Iceland: A potential monitoring tool. *Journal of Volcanology and Geothermal Research*  
526 289, 224–237. doi:10.1016/j.jvolgeores.2014.11.004.
- 527 Franco, L., Palma, J.L., Lara, L.E., Gil-Cruz, F., Cardona, C., Basualto, D., San Martín, J., 2019.  
528 Eruptive sequence and seismic activity of Llaima volcano (Chile) during the 2007–2009 eruptive period:  
529 Inferences of the magmatic feeding system. *Journal of Volcanology and Geothermal Research* 379,  
530 90–105. doi:10.1016/j.jvolgeores.2019.04.014.
- 531 Geller, R.J., Mueller, C.S., 1980. Four similar earthquakes in central California. *Geophysical Research*  
532 *Letters* 7, 821–824. doi:10.1029/GL007i010p00821.
- 533 Gärtner-Roer, I., Naegeli, K., Huss, M., Knecht, T., Machguth, H., Zemp, M., 2014. A database of  
534 worldwide glacier thickness observations. *Global and Planetary Change* 122, 330–344. doi:10.1016/j.  
535 gloplacha.2014.09.003.
- 536 Heap, M.J., Kennedy, B.M., Pernin, N., Jacquemard, L., Baud, P., Farquharson, J.I., Scheu, B., Lavallée,  
537 Y., Gilg, H.A., Letham-Brake, M., et al., 2015. Mechanical behaviour and failure modes in the  
538 Whakaari (White Island volcano) hydrothermal system, New Zealand. *Journal of Volcanology and*  
539 *Geothermal Research* 295, 26–42. doi:10.1016/j.jvolgeores.2015.02.012.
- 540 Iverson, R.M., Dzurisin, D., Gardner, C.A., Gerlach, T.M., LaHusen, R.G., Lisowski, M., Major, J.J.,  
541 Malone, S.D., Messerich, J.A., Moran, S.C., Pallister, J.S., Qamar, A.I., Schilling, S.P., Vallance, J.W.,  
542 2006. Dynamics of seismogenic volcanic extrusion at Mount St Helens in 2004-05. *Nature* 444, 439–43.  
543 doi:10.1038/nature05322.
- 544 Jónsdóttir, K., Roberts, R., Pohjola, V., Lund, B., Shomali, Z.H., Tryggvason, A., Böðvarsson, R.,  
545 Bövarsson, R., 2009. Glacial long period seismic events at Katla volcano, Iceland. *Geophysical*  
546 *Research Letters* 36, L11402. doi:10.1029/2009GL038234.
- 547 Kamb, B., 1970. Sliding motion of glaciers: Theory and observation. *Reviews of Geophysics* 8, 673.  
548 doi:10.1029/RG008i004p00673.
- 549 Kendrick, J.E., Lavallée, Y., Hirose, T., Di Toro, G., Hornby, A.J., De Angelis, S., Dingwell, D.B., 2014.  
550 Volcanic drumbeat seismicity caused by stick-slip motion and magmatic frictional melting. *Nature*  
551 *Geoscience* 7, 438–442. doi:10.1038/NGEO2146.
- 552 Kumagai, H., Nakano, M., Maeda, T., Yepes, H., Palacios, P., Ruiz, M., Arrais, S., Vaca, M., Molina,  
553 I., Yamashima, T., 2010. Broadband seismic monitoring of active volcanoes using deterministic and  
554 stochastic approaches. *Journal of Geophysical Research* 115, B08303. doi:10.1029/2009JB006889.
- 555 Lamb, O.D., De Angelis, S., Wall, R.J., Lamur, A., Varley, N.R., Reyes-Dávila, G.A., Arámbula-  
556 Mendoza, R., Hornby, A.J., Kendrick, J.E., Lavallée, Y., 2017. Seismic and experimental insights into  
557 eruption precursors at Volcán de Colima. *Geophysical Research Letters* 44, 6092–6100. doi:10.1002/  
558 2017GL073350.
- 559 Lamb, O.D., Lees, J., Marin, L.F., Lazo, J., Rivera, A., Shore, M., Lee, S., 2020. Investigating potential  
560 icequakes at Llaima volcano, Chile. *Volcanica* 3, 29–42. doi:10.30909/vol.03.01.2942.
- 561 Leet, R.C., 1988. Saturated and subcooled hydrothermal boiling in groundwater flow channels as a  
562 source of harmonic tremor. *Journal of Geophysical Research: Solid Earth* 93, 4835–4849. doi:10.1029/

563 JB093iB05p04835.

564 de Maisonneuve, C.B., Dungan, M.A., Bachmann, O., Burgisser, A., 2012. Insights into shallow magma  
565 storage and crystallization at Volcán Llaima (Andean Southern Volcanic Zone, Chile). *Journal of*  
566 *Volcanology and Geothermal Research* 211–212, 76–91. doi:[https://doi.org/10.1016/j.jvolgeores.](https://doi.org/10.1016/j.jvolgeores.2011.09.010)  
567 2011.09.010.

568 Matoza, R.S., Chouet, B.A., Dawson, P.B., Shearer, P.M., Haney, M.M., Waite, G.P., Moran, S.C.,  
569 Mikesell, T.D., 2015. Source mechanism of small long-period events at Mount St. Helens in July 2005  
570 using template matching, phase-weighted stacking, and full-waveform inversion. *Journal of Geophysical*  
571 *Research: Solid Earth* 120, 6351–6364. doi:10.1002/2015JB012279.

572 Matthews, A.J., Barclay, J., Johnstone, J.E., 2009. The fast response of volcano-seismic activity to intense  
573 precipitation: Triggering of primary volcanic activity by rainfall at Soufrière Hills Volcano, Montserrat.  
574 *Journal of Volcanology and Geothermal Research* 184, 405–415. doi:10.1016/j.jvolgeores.2009.05.  
575 010.

576 Mikesell, T.D., Wijk, K.V., Haney, M.M., Bradford, J.H., Marshall, H.P., Harper, J.T., 2012. Monitoring  
577 glacier surface seismicity in time and space using Rayleigh waves. *Journal of Geophysical Research*  
578 117, 1–12. doi:10.1029/2011JF002259.

579 Mora-Stock, C., Thorwart, M., Wunderlich, T., Bredemeyer, S., Hansteen, T.H., Rabbel, W., 2014.  
580 Comparison of seismic activity for Llaima and Villarrica volcanoes prior to and after the Maule 2010  
581 earthquake 103, 2015–2028. doi:10.1007/s00531-012-0840-x.

582 Métaixian, J.P., Araujo, S., Mora, M.M., Lesage, P., 2003. Seismicity related to the glacier of Cotopaxi  
583 Volcano, Ecuador. *Geophysical Research Letters* 30, 1–4. doi:10.1029/2002GL016773.

584 Nanni, U., Gimbert, F., Vincent, C., Gräff, D., Walter, F., Piard, L., Moreau, L., 2020. Quantification of  
585 seasonal and diurnal dynamics of subglacial channels using seismic observations on an Alpine glacier.  
586 *The Cryosphere* 14, 1475–1496. doi:10.5194/tc-14-1475-2020.

587 Naranjo, J.A., Moreno, H., 2005. *Geología del Volcán Llaima. Carta Geológica de Chile - Serie Geología*  
588 *Básica* 88, 1–37.

589 Park, I., Jolly, A., Kim, K.Y., Kennedy, B., 2019. Temporal variations of repeating low frequency volcanic  
590 earthquakes at Ngauruhoe Volcano, New Zealand. *Journal of Volcanology and Geothermal Research*  
591 373, 108–119. doi:10.1016/j.jvolgeores.2019.01.024.

592 Podolskiy, E.A., Fujita, K., Sunako, S., Sato, Y., 2019. Viscoelastic Modeling of Nocturnal Thermal  
593 Fracturing in a Himalayan Debris-Covered Glacier. *Journal of Geophysical Research: Earth Surface*  
594 124, 1485–1515. doi:10.1029/2018JF004848.

595 Podolskiy, E.A., Fujita, K., Sunako, S., Tsushima, A., Kayastha, R.B., 2018. Nocturnal Thermal  
596 Fracturing of a Himalayan Debris-Covered Glacier Revealed by Ambient Seismic Noise. *Geophysical*  
597 *Research Letters* 45, 9699–9709. doi:10.1029/2018GL079653.

598 Podolskiy, E.A., Walter, F., 2016. Cryoseismology. *Reviews of Geophysics* S4, 708–758. doi:10.1002/  
599 2016RG000526.

600 Reinthaler, J., Paul, F., Granados, H.D., Rivera, A., Huggel, C., 2019. Area changes of glaciers on active  
601 volcanoes in Latin America between 1986 and 2015 observed from multi-temporal satellite imagery.  
602 *Journal of Glaciology* , 1–15doi:10.1017/jog.2019.30.

603 Roeoesli, C., Helmstetter, A., Walter, F., Kissling, E., 2016. Meltwater influences on deep stick-slip  
604 icequakes near the base of the Greenland Ice Sheet. *Journal of Geophysical Research: Earth Surface*  
605 121, 223–240. doi:10.1002/2015JF003601.

606 Ruth, D.C.S., Costa, F., Bouvet de Maisonneuve, C., Franco, L., Cortés, J.A., Calder, E.S., 2018.  
607 Crystal and melt inclusion timescales reveal the evolution of magma migration before eruption. *Nature*  
608 *Communications* 9, 2657. doi:10.1038/s41467-018-05086-8.

609 Ruth, D.C.S., Cottrell, E., Calder, E.S., Cortés, J.A., Kelley, K.A., 2016. From Passive Degassing to

- 610 Violent Strombolian Eruption: the Case of the 2008 Eruption of Llaima Volcano, Chile. *Journal of*  
611 *Petrology* 57, 1833–1864. doi:10.1093/petrology/egw063.
- 612 Senobari, N.S., Funning, G.J., Keogh, E., Zhu, Y., Yeh, C.M., Zimmerman, Z., Mueen, A., 2019. Super-  
613 Efficient Cross-Correlation (SEC-C): A Fast Matched Filtering Code Suitable for Desktop Computers.  
614 *Seismological Research Letters* 90, 322–334. doi:10.1785/0220180122.
- 615 Thelen, W.A., Allstadt, K.E., De Angelis, S., Malone, S.D., Moran, S.C., Vidale, J., 2013. Shallow  
616 repeating seismic events under an alpine glacier at Mount Rainier, Washington, USA. *Journal of*  
617 *Glaciology* 59, 345–356. doi:10.3189/2013JoG12J111.
- 618 Venzke, E., 2013. Global Volcanism Program. doi:10.5479/si.GVP.V0TW4-2013.
- 619 Weaver, C.S., Malone, S.D., 1976. Mt. Saint Helens Seismic Events: Volcanic Earthquakes or Glacial  
620 Noises? *Geophysical Research Letters* 3, 197–200.
- 621 Weaver, C.S., Malone, S.D., 1979. Seismic evidence for discrete glacier motion at the rock-ice interface.  
622 *Journal of Glaciology* 23, 171–184. doi:10.1017/S0022143000029816.
- 623 Wech, A.G., Creager, K.C., 2008. Automated detection and location of Cascadia tremor. *Geophysical*  
624 *Research Letters* 35, L20302. doi:10.1029/2008GL035458.